144 *Biochemistry* **2011,** *50,* 144–150
DOI: 10.1021/bi101819m

BIOCHEMISTRY
including biophysical chemistry & molecular biology
Article

The Tightly Bound Calcium of MauG Is Required for Tryptophan Tryptophylquinone Cofactor Biosynthesis[†]

Sooim Shin,[‡] Manliang Feng,[‡] Yan Chen,[§] Lyndal M. R. Jensen,[∥] Hiroyasu Tachikawa,[⊥] Carrie M. Wilmot,[∥] Aimin Liu,[§] and Victor L. Davidson*[,‡]

[‡]*Department of Biochemistry, University of Mississippi Medical Center, Jackson, Mississippi 39216, United States,* [§]*Department of Chemistry, Georgia State University, Atlanta, Georgia 30302, United States,* [∥]*Department of Biochemistry, Molecular Biology and Biophysics, University of Minnesota, 321 Church Street SE, Minneapolis, Minnesota 55455, United States, and* [⊥]*Department of Chemistry, Jackson State University, Jackson, Mississippi 39217, United States*

Received November 12, 2010; Revised Manuscript Received December 3, 2010

ABSTRACT: The diheme enzyme MauG catalyzes a six-electron oxidation required for posttranslational modification of a precursor of methylamine dehydrogenase (preMADH) to complete the biosynthesis of its protein-derived tryptophan tryptophylquinone (TTQ) cofactor. The crystal structure of the MauG−preMADH complex revealed the presence of a Ca^{2+} in proximity to the two hemes [Jensen, L. M. R., Sanishvili, R., Davidson, V. L., and Wilmot, C. M. (2010) *Science 327*, 1392−1394]. This Ca^{2+} did not readily dissociate; however, after extensive treatment with EGTA or EDTA MauG was no longer able to catalyze TTQ biosynthesis and exhibited altered absorption and resonance Raman spectra. The changes in spectral features are consistent with Ca^{2+}-dependent changes in heme spin state and conformation. Addition of H_2O_2 to the Ca^{2+}-depleted MauG did not yield spectral changes characteristic of formation of the bis-Fe(IV) state which is stabilized in native MauG. After addition of Ca^{2+} to the Ca^{2+}-depleted MauG, full TTQ biosynthesis activity and reactivity toward H_2O_2 were restored, and the spectral properties returned to those of native MauG. Kinetic and equilibrium studies of Ca^{2+} binding to Ca^{2+}-depleted MauG indicated a two-step mechanism. Ca^{2+} initially reversibly binds to Ca^{2+}-depleted MauG (K_d = 22.4 μM) and is followed by a relatively slow ($k = 1.4 \times 10^{-3}$ s^{-1}) but highly favorable (K_{eq} = 4.2) conformational change, yielding an equilibrium dissociation constant $K_{d,eq}$ value of 5.3 μM. The circular dichroism spectra of native and Ca^{2+}-depleted MauG were essentially the same, consistent with Ca^{2+}-induced conformational changes involving domain or loop movements rather than general unfolding or alteration of secondary structure. These results are discussed in the context of the structures of MauG and heme-containing peroxidases.

Calcium participates in a variety of important biological functions, many of which are accomplished through interaction with proteins. Ca^{2+} binding allows muscle contraction through conformational transitions in troponin C (*1*). The calcium-binding protein calmodulin regulates a number of different protein targets, thereby affecting many different cellular functions (*2*). Ca^{2+} is required for the activity of enzymes such as phospholipase A_2 (*3*). Ca^{2+} has also been detected in heme-containing peroxidases of plants, fungi, bacteria, and animals, including canine myeloperoxidase (*4*), horseradish peroxidase (*5*, *6*), cationic peanut peroxidase (*7*), manganese peroxidase (*8*), lignin peroxidase (*9*), and bacterial diheme cytochrome *c* peroxidase (BCCP)[1] (*10*). In general, Ca^{2+} has been proposed to maintain a heme conformation and heme pocket structure associated with high catalytic activities for these peroxidases.

Bound Ca^{2+} has also been found in the crystal structure of the diheme enzyme MauG from *Paracoccus denitrificans* (*11*) (Figure 1). MauG exhibits approximately 30% sequence homology to BCCPs (*10*, *12*), and the crystal structures of MauG and various BCCPs reveal that the orientation of the Ca^{2+} and two hemes is essentially identical in the two classes of proteins (*10*, *11*, *13*). Despite this structural similarity, BCCPs and MauG exhibit significant differences in catalytic and redox behavior (*14*, *15*). MauG catalyzes the final steps in the biosynthesis of the protein-derived cofactor (*16*), tryptophan tryptophylquinone (TTQ) (*17*) in methylamine dehydrogenase (MADH). MauG catalyzes a six-electron oxidation of a precursor protein (preMADH) containing monohydroxylated βTrp57 (Scheme 1). During this process a second oxygen atom is inserted into the indole ring of βTrp57, βTrp57 is covalently cross-linked to βTrp108, and the quinol species is oxidized to the quinone. These reactions proceed via a high-valent bis-Fe(IV) redox state of MauG that may be generated by reaction of diferrous MauG with molecular oxygen or reaction of diferric MauG with H_2O_2 (*18*).

The role of Ca^{2+} in BCCPs has been extensively studied, and it has been found to be essential for activity (*10*). For most BCCPs the as-isolated enzyme is in an inactive diferric state in which the H_2O_2-binding heme is six-coordinate with His−His axial ligation (*19*). The reduction of the other heme in BCCP, which is six-coordinate with His−Met ligation, generates a mixed-valence

[†]This work was supported by NSF Grant MCB-0843537 (A.L.), NIH Grants GM-41574 (V.L.D.), RCMI G12RR13459 (H.T.), and GM-66569 (C.M.W.), and Minnesota Partnership for Biotechnology and Medical Genomics Grant SPAP-05-0013-P-FY06 (C.M.W.).

*Address correspondence to this author. Tel: 601-984-1516. Fax: 601-984-1501. E-mail: vdavidson@umc.edu.

[1]Abbreviations: MADH, methylamine dehydrogenase; TTQ, tryptophan tryptophylquinone; preMADH, the biosynthetic precursor protein of MADH with incompletely synthesized TTQ; BCCP, bacterial diheme cytochrome *c* peroxidase; ET, electron transfer; bis-Fe(IV) MauG, redox state of MauG with one heme as Fe(IV)=O and the other as Fe(IV); CD, circular dichroism.

 Published on Web 12/03/2010

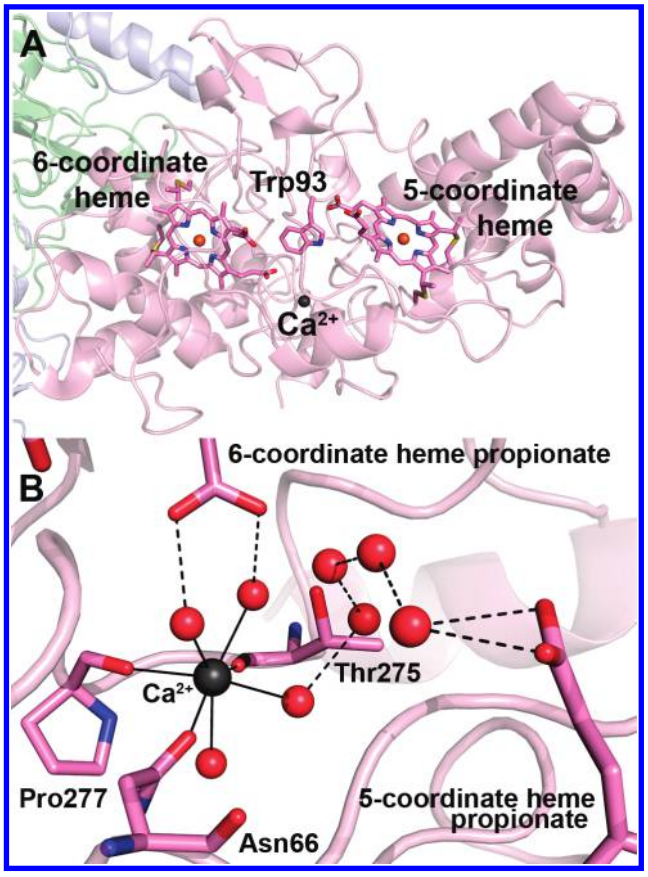

FIGURE 1: Structure of the Ca^{2+} site in MauG. (A) Secondary structure depiction of MauG in complex with preMADH. (B) Ca^{2+} ligation with closest heme contacts and mediating water networks. Color scheme is MauG (pink), preMADH α (blue), and preMADH *β* (green). The hemes, Trp93, and Ca^{2+} ligands of MauG are drawn explicitly in stick representation colored by atom. Ca^{2+}, iron, and water are represented by spheres colored black, orange, and red, respectively. Ca^{2+}−ligand bonds are represented as solid lines and hydrogen bonds as dashed lines. This figure was produced using PyMOL (http://www.pymol.org/) and Protein Data Bank entry 3L4M.

state that triggers a Ca^{2+}-dependent conformational change in which the distal His ligand of the H_2O_2-binding heme is replaced by water (*20*, *21*). This activated form of the enzyme then proceeds through its normal reaction cycle. Relaxation back to the fully oxidized inactive state only occurs when insufficient reductant is present, and therefore the diferric form is not considered part of the catalytic cycle of the BCCPs. MauG also has Ca^{2+} bound with identical ligation to that of BCCP, but in this case the diferric enzyme is active, and there is no evidence for the mixed-valence state that is central in the reaction cycle of BCCP. Thus while structurally conserved, the role of Ca^{2+} in MauG is clearly different from that in BCCP.

In this study we report methods to reversibly remove Ca^{2+} from MauG and reconstitute the Ca^{2+}-depleted MauG with Ca^{2+}. This allowed the characterization of the effects of Ca^{2+} on the physical and catalytic properties of MauG. The Ca^{2+}-depleted MauG is inactive in TTQ biosynthesis and exhibits altered spectral properties. The results reveal Ca^{2+}-dependent changes in heme spin state and heme conformation. These changes are reversible, as after incubation of Ca^{2+}-depleted MauG with Ca^{2+} the native spectral properties and activity are regained. The reconstitution with Ca^{2+} is shown to proceed via a two-step mechanism of reversible binding followed by a conformational change. MauG uses H_2O_2 to catalyze posttranslational modifications of a protein substrate, but it does not function primarily as a peroxidase. Despite this different reactivity, MauG shares the common feature of a bound Ca^{2+} in proximity to the heme(s) that is seen in *b*-type heme peroxidases and *c*-type diheme peroxidases. The effects of removal of Ca^{2+} from MauG on its spectroscopic and catalytic properties, and the mechanism of Ca^{2+} binding to Ca^{2+}-depleted MauG, are discussed and compared with studies of the roles of Ca^{2+} in peroxidases.

Scheme 1: Reactions Catalyzed by MauG

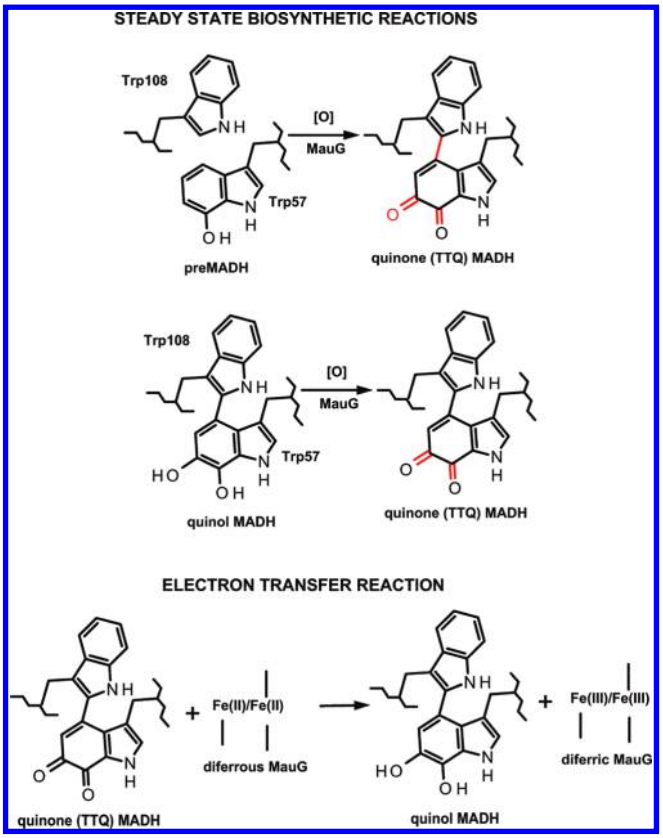

EXPERIMENTAL PROCEDURES

Protein Purification and Preparation. Methods for the expression and purification of MADH (*22*), preMADH (*23*), and MauG (*12*) were as described previously. Concentrations of these proteins were calculated using the following extinction coefficients: diferric MauG (ε_{406} = 309000 M^{-1} cm^{-1}), quinone MADH (ε_{440} = 26200 M^{-1} cm^{-1}), and quinol MADH (ε_{330} = 56400 M^{-1} cm^{-1}). Ca^{2+}-depleted MauG was prepared by incubation of native MauG with either 0.01 M EDTA disodium salt or EGTA in 0.01 M potassium phosphate buffer, pH 7.5, for 15 h at 4 °C. The chelator was removed, and the buffer was exchanged to 0.05 M Tris-HCl, pH 7.5, by centrifugation. Ca^{2+}-reconstituted MauG was prepared by incubation of Ca^{2+}-depleted MauG with 0.01 M $CaCl_2$ in 0.05 M Tris-HCl, pH 7.5. Reduction and oxidation of MauG proteins were performed anaerobically using sodium dithionite and potassium ferricyanide, respectively.

Spectrophotometric Assay of Ca^{2+}-Depleted MauG Activity. The activity of Ca^{2+}-depleted MauG was assayed in three different reactions, two involving TTQ biosynthesis and one involving only electron transfer (Scheme 1). Two steady-state spectrophotometric assays of MauG-dependent TTQ biosynthesis

using either preMADH (*14*) or quinol MADH (*24*) as the substrate were performed as described previously using H_2O_2 as the source of oxidizing equivalents. The single-turnover kinetics of the reaction of diferrous Ca^{2+}-depleted MauG with quinone MADH was also studied as described previously for native MauG (*24*).

Kinetic and Equilibrium Analysis of Ca^{2+} Binding to Ca^{2+}-Depleted MauG. Transient kinetic experiments of Ca^{2+} binding to Ca^{2+}-depleted MauG were performed using a Shimadzu Multispec-1501 spectrophotometer. A fixed concentration of 3 μM Ca^{2+}-depleted MauG was mixed with varied concentrations of $CaCl_2$ solution. The reaction was monitored by the rate of the spectral change corresponding to the return to the spectrum of diferric native MauG. Data were analyzed as described above using eqs 1 and 2, where E is the inactive Ca^{2+}-depleted MauG and E′ is the active Ca^{2+}-reconstituted MauG.

$$E + Ca^{2+} \overset{K_d}{\rightleftharpoons} E{-}Ca^{2+} \underset{k_4}{\overset{k_3}{\rightleftharpoons}} E' \quad (1)$$

$$k_{obs} = k_3[Ca^{2+}]/([Ca^{2+}] + K_d) + k_4 \quad (2)$$

The equilibrium binding of Ca^{2+} to Ca^{2+}-depleted MauG was also analyzed. $CaCl_2$ was added to Ca^{2+}-depleted MauG in increasing concentrations, and the magnitude of the Ca^{2+}-induced spectral change was recorded after the system had reached equilibrium. These data were analyzed using eq 3, where Y is the absorbance increase at 370 nm, and $K_{d,eq}$ is the apparent K_d value obtained from the equilibrium measurements.

$$Y = Y_{max}[Ca^{2+}]/(K_{d,eq} + [Ca^{2+}]) \quad (3)$$

Resonance Raman Spectroscopy. Resonance Raman spectra of MauG samples were recorded using a Raman spectrometer consisting of a Spex model 1877 triple spectrograph and a CCD detector as reported previously (*15*). A 406.7 nm line from an argon−krypton ion laser (Spectra-Physics BeamLok model 2080-KV) was used as the excitation source, and the Raman signal was collected in a 120° geometry. The laser power was adjusted to ~5 mW at the sample. Each spectrum was recorded with a 60 s accumulation time, and 10 repetitively measured spectra were averaged to improve the quality of the final spectrum. The wavenumbers of the Raman bands in the spectra of the samples were calibrated using the spectrum of cyclohexane as a standard. Samples contained 0.15 mM protein in 0.05 M Tris-HCl, pH 7.5, and spectra were recorded at 25 °C.

Circular Dichroism (CD) Spectroscopy. The CD spectra (190−250 nm) of native and Ca^{2+}-depleted MauG were acquired on a JASCO J-810 spectropolarimeter (JASCO, Easton, MD, USA) at ambient temperature. In each measurement, a MauG sample (7 μM) was placed in a 1 mm path length quartz cell in 0.05 M potassium phosphate, pH 7.5. All spectra were the average of at least 10 scans with a scan rate of 50 nm min^{-1}. The spectra were converted to the mean residue molar ellipticity θ_λ according to eq 4, where θ_{obs} is the average of measured ellipticity at λ nm, C is the molar concentration, L is the light path (cm), and N is the number of amino acids in the protein sequence.

$$\theta_\lambda = \frac{\theta_{obs}}{CLN} \quad (4)$$

RESULTS

Effects of Ca^{2+} on the Visible Absorption Spectrum of MauG. Comparison of the absorption spectra of the diferric native and diferric Ca^{2+}-depleted MauG (Figure 2A) reveals that the removal of Ca^{2+} results in a 4 nm red shift of the absorption maxima of the Soret peak and a narrowing of the peak width. In contrast, the absorption spectra of the diferrous native and diferrous Ca^{2+}-depleted MauG (Figure 2B) reveal that the positions of the α, β, and Soret peaks are very similar, although a slight narrowing of the Soret peak is observed after removal of Ca^{2+}. After reconstitution of Ca^{2+}-depleted MauG with Ca^{2+} the spectra of both diferric and diferrous Ca^{2+}-reconstituted MauG were essentially identical to the corresponding native MauG spectra (not shown).

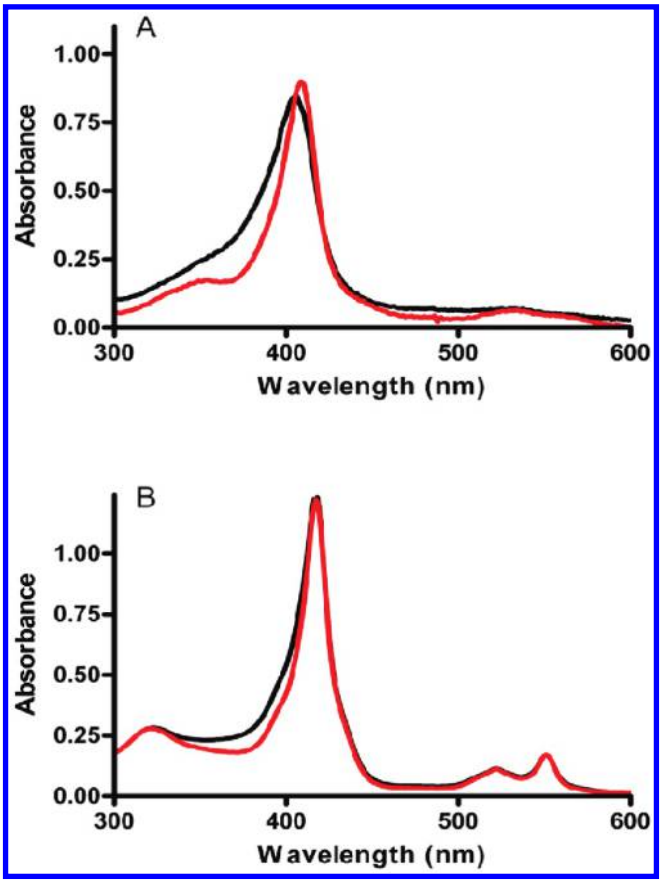

FIGURE 2: Effect of Ca^{2+} depletion on the absorption spectra of MauG. (A) Overlay of the absorption spectra of diferric native (black) and diferric Ca^{2+}-depleted (red) MauG. (B) Overlay of the absorption spectra of diferrous native (black) and diferrous Ca^{2+}-depleted (red) MauG.

Addition of H_2O_2 to native MauG results in formation of a relatively stable bis-Fe(IV) redox state which exhibits a decrease in the intensity of the Soret peak and a 2 nm red shift of the absorption maxima. This bis-Fe(IV) species slowly spontaneously decays back to the diferric state over several minutes (*18*, *25*). When H_2O_2 was added to Ca^{2+}-depleted MauG, a decrease in the intensity of the Soret peak was observed without an accompanying red shift (Figure 3). In contrast to native MauG this spectral change did not spontaneously return to the initial spectrum, but instead the intensity of the Soret peak continued to slowly decrease over several minutes. Thus, there is no evidence that Ca^{2+}-depleted MauG is able to stabilize the bis-Fe(IV) redox state. When this experiment was repeated with Ca^{2+}-reconstituted MauG, the spectral changes and rate of spontaneous decay back to the diferric state were identical to those of native MauG (not shown).

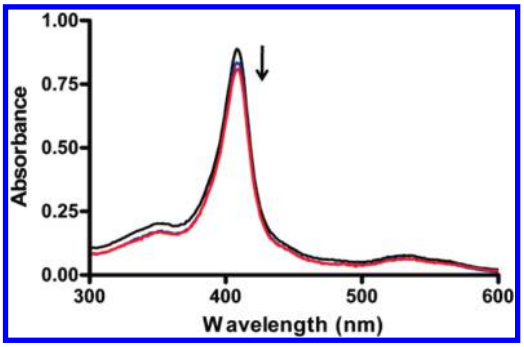

FIGURE 3: Changes in the absorption spectrum of Ca^{2+}-depleted MauG upon addition of H_2O_2. Spectra were obtained before (black), immediately after addition of an equivalent of H_2O_2 (blue), and 10 min after addition of H_2O_2 (red) to Ca^{2+}-depleted MauG.

Effects of Ca^{2+} on the Resonance Raman Spectrum of MauG. Comparison of the resonance Raman spectra of the diferric native MauG and Ca^{2+}-depleted MauG revealed that the frequencies of several of the vibration modes are Ca^{2+}-dependent. The high-frequency region of the spectra (Figure 4A) contains several marker bands that are sensitive to oxidation state, spin state, and the conformation of the heme macrocycle (*26*−*28*). The assignment of marker bands is based on the work of Spiro and co-workers (*26*). The oxidation state marker band (ν_4) is centered at 1374 cm^{-1} in both spectra, indicating the presence of ferric state hemes. Native MauG contains a five-coordinate His-ligated high-spin heme and a six-coordinate His-Tyr-ligated low-spin heme (*11*). The native MauG spectrum contains ν_2 bands at 1571 (high spin) and 1587 cm^{-1} (low spin) and ν_3 bands at 1478 (high spin) and 1501 cm^{-1} (low spin). In the spectrum of Ca^{2+}-depleted MauG, only low-spin hemes are present, as evidenced by the loss of the high-spin marker bands at 1571 and 1478 cm^{-1}. The ν_{10} band in Ca^{2+}-depleted MauG has also shifted to higher frequency relative to native MauG, indicating a more planar heme macrocycle (*28*, *29*).

The low-frequency regions of the spectra (Figure 4B) also show Ca^{2+}-dependent changes. These bands originate from the in-plane and out-of-plane deformation modes of the porphyrin ring as well as the vibration modes from the heme substituents (*27*). Although there is considerable overlap of the bands in this region, frequency changes are clearly discernible. One of the major changes is to the δ ($C_\beta C_\alpha S$) mode, which shifts from 393 cm^{-1} in native MauG to 408 cm^{-1} in Ca^{2+}-depleted MauG. The vibration mode from the thioether bridge (ν(C−S)) which overlaps the ν_7 mode also shifts from 694 cm^{-1} in native MauG to 691 cm^{-1} in Ca^{2+}-depleted MauG. These changes suggest conformational changes impacting the thioether bridges which may originate from Ca^{2+}-dependent conformational changes of the protein backbone.

Effect of Ca^{2+} on MauG-Dependent TTQ Biosynthesis Activity and Interprotein Electron Transfer Reactivity. The activity of Ca^{2+}-depleted MauG was assayed in three different reactions, two involving TTQ biosynthesis and one involving only electron transfer (Scheme 1). Using spectroscopic steady-state assays in which native MauG has been shown to catalyze TTQ biosynthesis with either preMADH or quinol MADH as a substrate (*24*, *25*), no detectable TTQ biosynthesis activity was observed for Ca^{2+}-depleted MauG. After reincorporation of Ca^{2+}, the reconstituted MauG exhibited normal TTQ biosynthesis activity with both substrates. The k_{cat} values for the reaction of native and Ca^{2+}-reconstituted MauG with quinol MADH

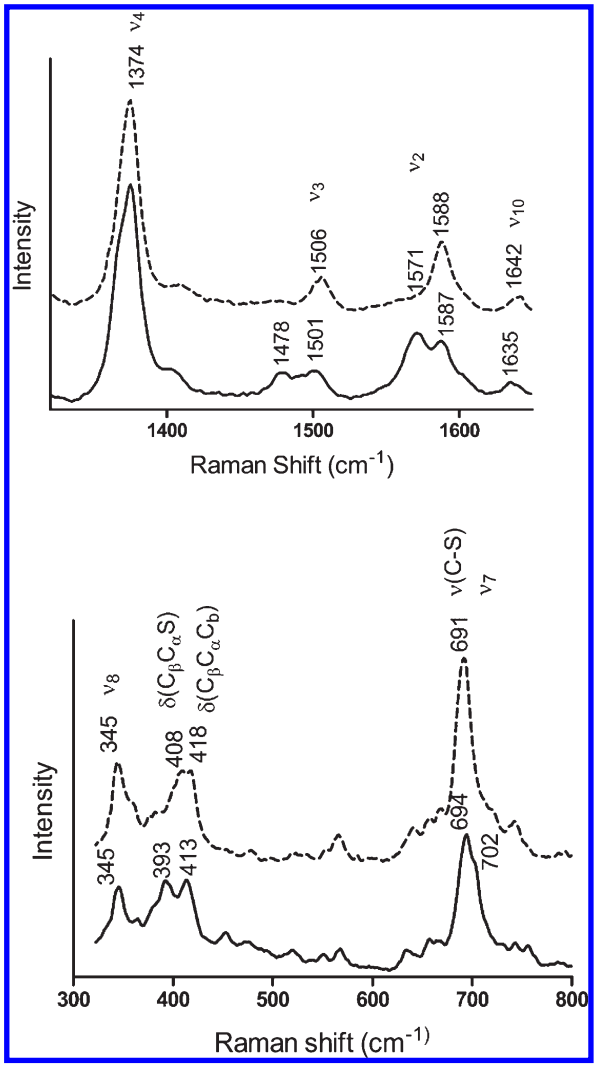

FIGURE 4: Effect of Ca^{2+} depletion on the resonance Raman spectrum of MauG. Overlay of the spectra of diferric native MauG (solid line) and Ca^{2+}-depleted MauG (dashed line) in the high-frequency (A, top panel) and low-frequency (B, bottom panel) regions. Relevant marker bands and their frequencies are indicated.

were 4.4 ± 0.1 and 4.3 ± 0.1 s^{-1}, respectively. The k_{cat} values for the reaction of native and Ca^{2+}-reconstituted MauG with preMADH were 0.10 ± 0.01 and 0.09 ± 0.01 s^{-1}, respectively.

Native MauG also exhibits activity in an electron transfer reaction from diferrous MauG to quinone MADH (Scheme 1). This reaction is thermodynamically favorable and does not require formation of a bis-Fe(IV) state, as do the TTQ biosynthetic reactions. In this reaction native MauG exhibits saturation behavior and a limiting first-order rate constant of 0.07 s^{-1} and K_d for complex formation with MADH of 10.1 μM (*24*). Ca^{2+}-depleted MauG did exhibit activity in this reaction. However, in this case the observed rate exhibited a linear dependence on quinone MADH concentration (Figure 5) and a bimolecular rate constant of (6.8 ± 0.4) × 10^2 M^{-1} s^{-1}, suggesting that formation of the protein−protein complex is the rate-limiting step. As the site of interaction with MADH is 19.4 Å from the nearest heme iron of MauG (*11*), this result suggests that the presence or absence of Ca^{2+} exerts an effect on the global conformation of MauG.

Kinetic and Equilibrium Analysis of Ca^{2+} Binding to Ca^{2+}-Depleted MauG. Addition of $CaCl_2$ to Ca^{2+}-depleted MauG results in a change in the absorption spectrum back to that characteristic of native diferric MauG (Figure 6A). To determine

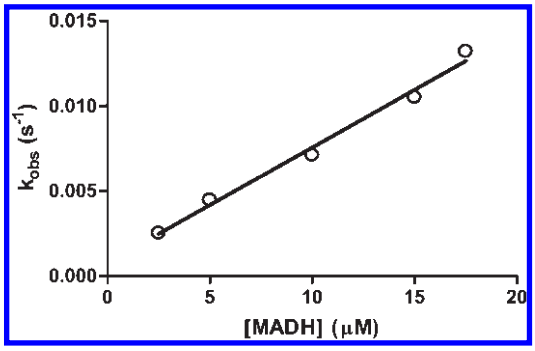

FIGURE 5: Concentration dependence of the rate of reaction of quinone MADH with diferrous Ca^{2+}-depleted MauG. The line shows the linear regression fit of the data.

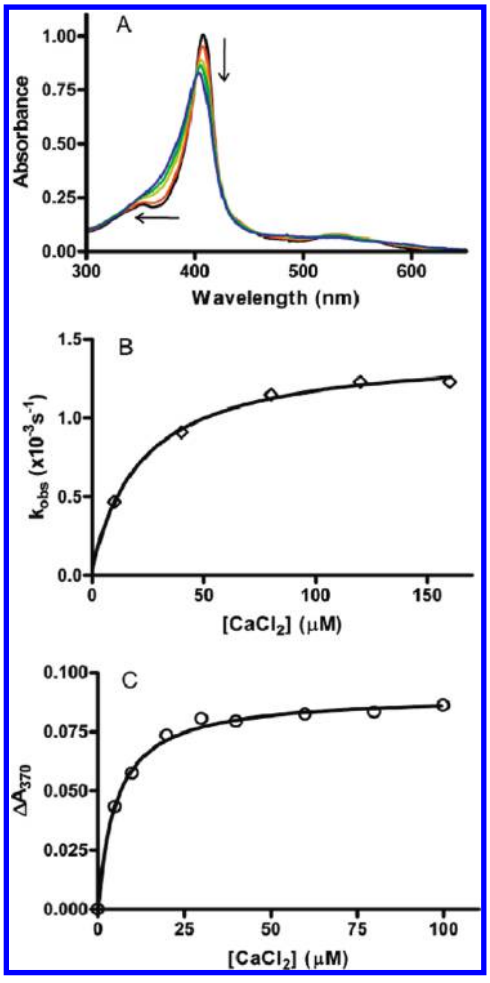

FIGURE 6: Binding of Ca^{2+} to Ca^{2+}-depleted MauG. (A) Changes in the absorption spectrum of Ca^{2+}-depleted MauG after addition of 0.5 mM $CaCl_2$. The spectra were recorded every 2 min after adding $CaCl_2$. The arrows show the direction of the absorbance changes. (B) Kinetic analysis of Ca^{2+} binding. Ca^{2+}-depleted MauG was mixed with varied concentrations of $CaCl_2$, and the rate of the spectral change was monitored. The line is a fit of the data to eq 2. (C) Equilibrium binding of Ca^{2+} to Ca^{2+}-depleted MauG. $CaCl_2$ was added to Ca^{2+}-depleted MauG in increasing concentrations, and the magnitude of the Ca^{2+}-induced spectral change was recorded after the system had reached equilibrium. The line is a fit of the data to eq 3.

the kinetic mechanism and kinetic parameters for Ca^{2+} binding, Ca^{2+}-depleted MauG was mixed with varied concentrations of $CaCl_2$, and the rate of the spectral change was monitored. Saturation behavior was observed (Figure 6B), and a two-step mechanism was required to explain the data (eqs 1 and 2). This

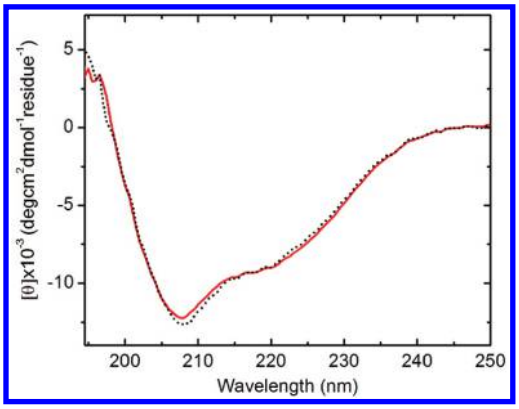

FIGURE 7: Effect of Ca^{2+} depletion on the circular dichroism spectrum of MauG. CD spectra of native (dotted black trace) and Ca^{2+}-depleted (solid red trace) MauG were recorded in 0.05 M potassium phosphate, pH 7.5.

yielded a limiting first-order rate constant (k_3) of $(1.4 \pm 0.1) \times 10^{-3}$ s^{-1} and a K_d ($1/K_a$) value of 22.4 ± 7.9 μM. The requirement for a two-step mechanism for Ca^{2+} binding is significant, and the most likely explanation is that the absorbance change is a consequence of a relatively slow conformational change that is triggered by Ca^{2+} binding. The equilibrium binding of Ca^{2+} to Ca^{2+}-depleted MauG was also analyzed (Figure 6C), and the fit of the data to eq 3 yielded an equilibrium dissociation constant ($K_{d,eq}$) of 5.3 ± 0.3 μM. The discrepancy between the kinetically determined K_d value and that obtained by equilibrium binding reflects the fact that the binding event is not a simple single step mechanism but a two-step process. The kinetically determined K_d value of 22.4 μM describes the reversible binding of Ca^{2+} to Ca^{2+}-depleted MauG. The $K_{d,eq}$ value of 5.3 μM is the concentration at which 50% of the protein has bound Ca^{2+} under equilibrium conditions. As this process involves two consecutive reversible steps (see eq 1), the overall equilibrium binding constant will be a product of the equilibrium constants for each of the two steps (eq 5)

$$K_{d,eq} = K_d(k_4/k_3) \text{ or } K_{a,eq} = K_a(k_3/k_4) \quad (5)$$

expressed either in terms of an equilibrium dissociation constant $K_{d,eq}$ or an equilibrium association constant $K_{a,eq}$. Given the experimentally determined values of $K_d = 22.4$ μM and $K_{d,eq} = 5.3$ μM, one can calculate the equilibrium constant that describes the relatively slow conformational change that follows binding to be $K_{eq} = k_3/k_4 = 4.2$. Thus, while relatively slow, this conformational change is highly favorable.

Protein Secondary Structure. To examine the structural changes caused by Ca^{2+} depletion of MauG, the CD spectra of both native and Ca^{2+}-depleted MauG were obtained under identical conditions. Figure 7 shows that these spectra are nearly identical, suggesting that there was not a significant change in secondary structure. Thus, the depletion of Ca^{2+} from MauG must cause loop or domain movements rather than more extensive protein unfolding.

DISCUSSION

A common feature of several peroxidases is the presence of bound Ca^{2+} in the proximity of the heme(s). This is seen in both monoheme peroxidases with *b*-type hemes and in diheme peroxidases possessing *c*-type hemes. With the monoheme peroxidases the Ca^{2+} is strongly bound and does not dissociate under conditions in which the protein remains folded. For BCCP, which

contains two *c*-type hemes, Ca^{2+} can dissociate in the absence of chelators resulting in an inactive enzyme under physiological conditions and in so doing regulates its activity. Ca^{2+} binding converts the enzyme from an inactive form to an active mixed-valence form (*20*, *30*). The observed spectroscopic changes upon reduction of the inactive diferric to the active mixed-valence state of BCCP are consistent with the structurally characterized loss of the distal His ligand at the H_2O_2-binding heme (*19*−*21*). MauG possesses two *c*-type hemes and exhibits sequence and structural similarity to BCCPs, and the position and ligation of Ca^{2+} are identical (Figure 1) (*11*). However, diferric MauG already has an open distal site at the H_2O_2-binding heme, which structurally makes it more aligned with the active mixed-valence state of BCCP. Interestingly, the *Nitrosomonas europaea* BCCP, which of the characterized BCCPs has the most sequence identity to MauG (28%), is active in both the diferric and mixed-valence states (*31*). Unlike the crystal structures of other diferric BCCPs, the *N. europaea* diferric BCCP has an open distal site for H_2O_2-binding analogous to MauG (*13*). Thus, this BCCP may represent an evolutionary link between BCCPs and MauG.

The Ca^{2+}-binding site in MauG is located between the two hemes and close to Trp93 (Figure 1A). A similarly placed Trp is present in the BCCP structures and has been suggested to mediate electron transfer between hemes in that class of enzyme (*32*). The orientations of the two hemes, Trp93, and Ca^{2+} with respect to each other are essentially the same in the MauG and BCCP structures. In MauG, Ca^{2+} is coordinated to four water molecules, the main-chain carbonyl oxygen atoms of Thr275 and Pro277 and the oxygen of the Asn66 side chain forming a distorted pentagonal bipyramidal geometry (Figure 1B), which is identical to that observed in BCCP. The propionate A carboxylate oxygens of the six-coordinate His-Tyr-ligated heme are hydrogen bonded to two of the waters that provide Ca^{2+} ligands, and this feature is invariant in all crystal structures of BCCPs and MauG (Figure 1B) (*13*, *19*−*21*, *32*, *33*). This interaction has been postulated to modulate the pK_a of the heme propionate A of BCCP such that it remains deprotonated (*20*). The Ca^{2+} coordination sphere is unusual in having no carboxylate ligands from Asp or Glu residues, and this might also contribute to the propionate pK_a. In the proposed redox-coupled Bohr effect mechanism for BCCP only propionate D of the six-coordinate His-Met-ligated heme (analogous to His-Tyr in MauG) is capable of taking up a proton upon reduction. This leads to the breakage of a hydrogen bond to a main-chain amide that propagates large conformational changes resulting in the dissociation of the distal His of the H_2O_2-binding heme (*20*, *21*). However, in oxidized MauG and *N. europaea* BCCP there is no distal His present at this heme, and they adopt the propionate D conformer of the mixed-valence state of other BCCPs and consequently are catalytically competent in the diferric state (*11*, *13*). It is noteworthy that both hemes of MauG are linked to the Ca^{2+} via hydrogen-bonded waters (Figure 1B), since removal of Ca^{2+} from MauG causes alterations in the properties of both hemes.

The results of this study demonstrate that Ca^{2+}-dependent conformational changes in MauG affect its spectroscopic properties and that the bound Ca^{2+} is critical for the unusual catalytic properties of MauG. This indicates that the environment and conformation of the high-spin heme are significantly altered when Ca^{2+} is removed from MauG. These changes are reversible and consequently not the result of damage to the protein during the Ca^{2+} removal protocol. While inactive in the TTQ biosynthetic reactions which require the bis-Fe(IV) redox state, Ca^{2+}-depleted MauG was still redox active and able to transfer electrons to quinone MADH in a previously characterized nonbiosynthetic reaction (*24*). Whereas the kinetics of this reaction with native MauG exhibit saturation behavior, the reaction with Ca^{2+}-depleted MauG exhibited a linear dependence on quinone MADH concentration. This indicates that, after Ca^{2+} depletion, formation of the protein−protein complex is the rate-limiting step. This is consistent with the result suggesting a Ca^{2+}-dependent change in protein conformation. In this case, the Ca^{2+} depletion seems to have affected the MADH-binding site which is located > 30 Å from the H_2O_2-binding heme (*11*), suggesting that the structural influence of bound Ca^{2+} is propagated over a long distance through the protein. A Ca^{2+}-induced conformational change is additionally indicated by the results of the kinetic and equilibrium studies of Ca^{2+} binding to the Ca^{2+}-depleted MauG. The observed saturation behavior in the kinetic studies (hyperbolic concentration dependence of rate) requires a two-step mechanism for Ca^{2+} binding to Ca^{2+}-depleted MauG in which initially Ca^{2+} reversibly binds to Ca^{2+}-depleted MauG followed by a relatively slow but highly favorable conformational change that prevents the Ca^{2+} from readily dissociating. This conformational change is also reversible, but dissociation of Ca^{2+} can only occur from the unfavorable conformation which explains why prolonged incubation with a strong chelator is required to remove it from MauG.

The precise nature of the conformational change in MauG which is caused by removal of Ca^{2+} is not known, but the CD spectra are consistent with retention of the native protein secondary structure, indicating that significant protein unfolding is not occurring upon Ca^{2+} depletion. The observation that only low-spin hemes are observed in the resonance Raman spectrum of Ca^{2+}-depleted MauG suggests that an amino acid residue has moved to enable it to provide a distal ligand to the heme which is five-coordinate in native MauG. The more planar structure of the heme macrocycle evidenced in these data is also consistent with a change in coordination and could be a consequence of an easing of constraints on the porphyrin ring. Resonance Raman studies of Ca^{2+} binding to both the oxidized and mixed-valence states of BCCP from *Paracoccus pantotrophus* also suggested that upon Ca^{2+} depletion there was conversion of the five-coordinate high-spin heme to a six-coordinate low-spin heme (*29*, *30*). In BCCPs the residue which provides this removable distal ligand is a His. The conformation of the structural loop in the four crystal structures of BCCPs with dissociated His is very similar to that observed in MauG (*11*, *13*, *19*, *21*). However, in contrast to the BCCPs, the MauG loop does not contain a His, with Asp57 found at this position. Additional Asp, Glu, and Met residues are located within 10 Å of the heme Fe in the native MauG structure, and so the identification of the sixth heme ligand is not known. Thus far, it has not been possible to crystallize the Ca^{2+}-depleted MauG, and further spectroscopic and structural studies are in progress to try to identify the residue which provides the distal ligand in Ca^{2+}-depleted MauG and the nature of the accompanying structural change.

While calcium plays several critical functions in nature, its role in peroxidase function has received relatively little attention, with the BCCP being the best characterized (discussed earlier). It is clear that tightly bound Ca^{2+} is critical for the activity of a variety of other peroxidases. Horseradish peroxidase binds two Ca^{2+} which are required to maintain the structural integrity of the heme, for which the geometry for catalysis is lost upon Ca^{2+} removal (*5*, *6*). In cationic peanut peroxidase Ca^{2+} is believed to

position a catalytically important amino acid around the heme group which also affects the orientation of the porphyrin ring (*7*). For manganese peroxidase and lignin peroxidase it has been demonstrated that thermal inactivation which causes distinct alterations in the heme environment, change in heme spin state and changes in overall protein structure, is prevented and reversed in the presence of Ca^{2+} (*8*, *9*). In contrast to the peroxidases, heme-dependent oxygenases and oxidases do not typically contain bound Ca^{2+}. While the Ca^{2+}-binding sites of the monoheme and diheme peroxidases are different, the common feature of Ca^{2+} suggests that its role is specific to reaction of the heme with peroxide rather than a role in binding and activating molecular oxygen. MauG does not function primarily as a peroxidase but can use H_2O_2 to catalyze posttranslational modifications of its protein substrate. This suggests that MauG may have originally been a peroxidase and then evolved to acquire its new function. The findings reported here expand the scope of heme-dependent enzymes in which Ca^{2+} plays an important role.

ACKNOWLEDGMENT

We thank Yu Tang for technical assistance.

REFERENCES

1. Gagne, S. M., Tsuda, S., Li, M. X., Smillie, L. B., and Sykes, B. D. (1995) Structures of the troponin C regulatory domains in the apo and calcium-saturated states. *Nat. Struct. Biol. 2*, 784–789.
2. Tanaka, T., Umekawa, H., Saitoh, M., Ishikawa, T., Shin, T., Ito, M., Itoh, H., Kawamatsu, Y., Sugihara, H., and Hidaka, H. (1986) Modulation of calmodulin function and of Ca^{2+}-induced smooth muscle contraction by the calmodulin antagonist, HT-74. *Mol. Pharmacol. 29*, 264–249.
3. Murakami, M., and Kudo, I. (2002) Phospholipase A_2. *J. Biochem. 131*, 285–292.
4. Zeng, J., and Fenna, R. E. (1992) X-ray crystal structure of canine myeloperoxidase at 3Å resolution. *J. Mol. Biol. 226*, 185–207.
5. Laberge, M., Huang, Q., Schweitzer-Stenner, R., and Fidy, J. (2003) The endogenous calcium ions of horseradish peroxidase C are required to maintain the functional nonplanarity of the heme. *Biophys. J. 84*, 2542–2552.
6. Howes, B. D., Feis, A., Raimondi, L., Indiani, C., and Smulevich, G. (2001) The critical role of the proximal calcium ion in the structural properties of horseradish peroxidase. *J. Biol. Chem. 276*, 40704–40711
7. Barber, K. R., Rodriguez Maranon, M. J., Shaw, G. S., and Van Huystee, R. B. (1995) Structural influence of calcium on the heme cavity of cationic peanut peroxidase as determined by ^{1}H-NMR spectroscopy. *Eur. J. Biochem. 232*, 825–833.
8. Sutherland, G. R., Zapanta, L. S., Tien, M., and Aust, S. D. (1997) Role of calcium in maintaining the heme environment of manganese peroxidase. *Biochemistry 36*, 3654–3662.
9. Poulos, T. L., Edwards, S. L., Wariishi, H., and Gold, M. H. (1993) Crystallographic refinement of lignin peroxidase at 2Å. *J. Biol. Chem. 268*, 4429–4440.
10. Pettigrew, G. W., Echalier, A., and Pauleta, S. R. (2006) Structure and mechanism in the bacterial dihaem cytochrome *c* peroxidases. *J. Inorg. Biochem. 100*, 551–567.
11. Jensen, L. M., Sanishvili, R., Davidson, V. L., and Wilmot, C. M. (2010) In crystallo posttranslational modification within a MauG/pre-methylamine dehydrogenase complex. *Science 327*, 1392–1394.
12. Wang, Y., Graichen, M. E., Liu, A., Pearson, A. R., Wilmot, C. M., and Davidson, V. L. (2003) MauG, a novel diheme protein required for tryptophan tryptophylquinone biogenesis. *Biochemistry 42*, 7318–7325.
13. Shimizu, H., Schuller, D. J., Lanzilotta, W. N., Sundaramoorthy, M., Arciero, D. M., Hooper, A. B., and Poulos, T. L. (2001) Crystal structure of *Nitrosomonas europaea* cytochrome *c* peroxidase and the structural basis for ligand switching in bacterial di-heme peroxidases. *Biochemistry 40*, 13483–13490.
14. Li, X., Jones, L. H., Pearson, A. R., Wilmot, C. M., and Davidson, V. L. (2006) Mechanistic possibilities in MauG-dependent tryptophan tryptophylquinone biosynthesis. *Biochemistry 45*, 13276–13283.
15. Li, X., Feng, M., Wang, Y., Tachikawa, H., and Davidson, V. L. (2006) Evidence for redox cooperativity between *c*-type hemes of MauG which is likely coupled to oxygen activation during tryptophan tryptophylquinone biosynthesis. *Biochemistry 45*, 821–828.
16. Davidson, V. L. (2007) Protein-derived cofactors. Expanding the scope of post-translational modifications. *Biochemistry 46*, 5283–5292.
17. McIntire, W. S., Wemmer, D. E., Chistoserdov, A., and Lidstrom, M. E. (1991) A new cofactor in a prokaryotic enzyme: Tryptophan tryptophylquinone as the redox prosthetic group in methylamine dehydrogenase. *Science 252*, 817–824.
18. Li, X., Fu, R., Lee, S., Krebs, C., Davidson, V. L., and Liu, A. (2008) A catalytic di-heme *bis*-Fe(IV) intermediate, alternative to an Fe(IV)═O porphyrin radical. *Proc. Natl. Acad. Sci. U.S.A. 105*, 8597–8600.
19. Fulop, V., Ridout, C. J., Greenwood, C., and Hajdu, J. (1995) Crystal structure of the di-haem cytochrome *c* peroxidase from *Pseudomonas aeruginosa*. *Structure 3*, 1225–1233.
20. Echalier, A., Brittain, T., Wright, J., Boycheva, S., Mortuza, G. B., Fulop, V., and Watmough, N. J. (2008) Redox-linked structural changes associated with the formation of a catalytically competent form of the diheme cytochrome *c* peroxidase from *Pseudomonas aeruginosa*. *Biochemistry 47*, 1947–1956.
21. Echalier, A., Goodhew, C. F., Pettigrew, G. W., and Fulop, V. (2006) Activation and catalysis of the di-heme cytochrome *c* peroxidase from *Paracoccus pantotrophus*. *Structure 14*, 107–117.
22. Davidson, V. L. (1990) Methylamine dehydrogenases from methylotrophic bacteria. *Methods Enzymol. 188*, 241–246.
23. Pearson, A. R., De La Mora-Rey, T., Graichen, M. E., Wang, Y., Jones, L. H., Marimanikkupam, S., Agger, S. A., Grimsrud, P. A., Davidson, V. L., and Wilmot, C. M. (2004) Further insights into quinone cofactor biogenesis: Probing the role of MauG in methylamine dehydrogenase tryptophan tryptophylquinone formation. *Biochemistry 43*, 5494–5502.
24. Shin, S., Abu Tarboush, N., and Davidson, V. L. (2010) Long-range electron transfer reactions between hemes of MauG and different forms of tryptophan tryptophylquinone of methylamine dehydrogenase. *Biochemistry 49*, 5810–5816.
25. Lee, S., Shin, S., Li, X., and Davidson, V. (2009) Kinetic mechanism for the initial steps in MauG-dependent tryptophan tryptophylquinone biosynthesis. *Biochemistry 48*, 2442–2447.
26. Hu, S., Morris, I. K., Singh, J. P., Smith, K. M., and Spiro, T. G. (1993) Complete assignment of cytochrome *c* resonance Raman spectra via enzymatic reconstitution with isotopically labeled heme. *J. Am. Chem. Soc. 115*, 12446–12458.
27. Tu, A. T. (1982) in Raman spectroscopy in biology; principles and applications, pp 331−337, John Wiley and Sons, New York.
28. Desbois, A. (1994) Resonance Raman spectroscopy of *c*-type cytochromes. *Biochimie 76*, 693–707.
29. Pauleta, S. R., Lu, Y., Goodhew, C. F., Moura, I., Pettigrew, G. W., and Shelnutt, J. A. (2001) Calcium-dependent conformation of a heme and fingerprint peptide of the diheme cytochrome *c* peroxidase from *Paracoccus pantotrophus*. *Biochemistry 40*, 6570–6579.
30. Pauleta, S. R., Lu, Y., Goodhew, C. F., Moura, I., Pettigrew, G. W., and Shelnutt, J. A. (2008) Calcium-dependent heme structure in the reduced forms of the bacterial cytochrome *c* peroxidase from *Paracoccus pantotrophus*. *Biochemistry 47*, 5841–5850.
31. Arciero, D. M., and Hooper, A. B. (1994) A di-heme cytochrome *c* peroxidase from *Nitrosomonas europaea* catalytically active in both the oxidized and half-reduced states. *J. Biol. Chem. 269*, 11878–11886.
32. De Smet, L., Savvides, S. N., Van Horen, E., Pettigrew, G., and Van Beeumen, J. J. (2006) Structural and mutagenesis studies on the cytochrome *c* peroxidase from *Rhodobacter capsulatus* provide new insights into structure-function relationships of bacterial di-heme peroxidases. *J. Biol. Chem. 281*, 4371–4379.
33. Dias, J. M., Alves, T., Bonifacio, C., Pereira, A. S., Trincao, J., Bourgeois, D., Moura, I., and Romao, M. J. (2004) Structural basis for the mechanism of Ca^{2+} activation of the di-heme cytochrome *c* peroxidase from *Pseudomonas nautica 617*. *Structure 12*, 961–973.